# UC Irvine
## UC Irvine Previously Published Works

### Title
Cloud Activating Properties of Aerosol Observed during CELTIC

### Permalink
https://escholarship.org/uc/item/0ss6t67g

### Journal
Journal of the Atmospheric Sciences, 64(2)

### ISSN
0022-4928

### Authors
Stroud, Craig A
Nenes, Athanasios
Jimenez, Jose L
et al.

### Publication Date
2007-02-01

### DOI
10.1175/jas3843.1

### Copyright Information
This work is made available under the terms of a Creative Commons Attribution License, availalbe at https://creativecommons.org/licenses/by/4.0/

Peer reviewed

eScholarship.org Powered by the California Digital Library
University of California

# Cloud Activating Properties of Aerosol Observed during CELTIC

CRAIG A. STROUD,*,** ATHANASIOS NENES,+ JOSE L. JIMENEZ,#,@ PETER F. DECARLO,@,& J. ALEX HUFFMAN,#,@ ROELOF BRUINTJES,* EIKO NEMITZ,*,++ ALICE E. DELIA,&,## DARIN W. TOOHEY,& ALEX B. GUENTHER,* AND SREELA NANDI*

* *National Center for Atmospheric Research, Boulder, Colorado*
+ *School of Earth and Atmospheric Sciences, and Chemical and Biomolecular Engineering, Georgia Institute of Technology, Atlanta, Georgia*
# *Department of Chemistry and Biochemistry, Boulder, Colorado*
@ *Cooperative Institute for Research in the Environmental Sciences, Boulder, Colorado*
& *Program in Atmospheric and Oceanic Sciences, University of Colorado, Boulder, Colorado*

(Manuscript received 14 July 2005, in final form 8 February 2006)

ABSTRACT

Measurements of aerosol size distribution, chemical composition, and cloud condensation nuclei (CCN) concentration were performed during the Chemical Emission, Loss, Transformation, and Interactions with Canopies (CELTIC) field program at Duke Forest in North Carolina. A kinetic model of the cloud activation of ambient aerosol in the chamber of the CCN instrument was used to perform an aerosol–CCN closure study. This study advances prior investigations by employing a novel fitting algorithm that was used to integrate scanning mobility particle sizer (SMPS) measurements of aerosol number size distribution and aerosol mass spectrometer (AMS) measurements of the mass size distribution for sulfate, nitrate, ammonium, and organics into a single, coherent description of the ambient aerosol in the size range critical to aerosol activation (around 100-nm diameter). Three lognormal aerosol size modes, each with a unique internally mixed composition, were used as input into the kinetic model. For the two smaller size modes, which control CCN number concentration, organic aerosol mass fractions for the defined cases were between 58% and 77%. This study is also unique in that the water vapor accommodation coefficient was estimated based on comparing the initial timing for CCN activation in the instrument chamber with the activation predicted by the kinetic model. The kinetic model overestimated measured CCN concentrations, especially under polluted conditions. Prior studies have attributed a positive model bias to an incomplete understanding of the aerosol composition, especially the role of organics in the activation process. This study shows that including measured organic mass fractions with an assumed organic aerosol speciation profile (pinic acid, fulvic acid, and levoglucosan) and an assumed organic aerosol solubility of 0.02 kg kg$^{-1}$ still resulted in a significant model positive bias for polluted case study periods. The slope and $y$ intercept for the CCN predicted versus CCN observed regression was found to be 1.9 and $-180$ cm$^{-3}$, respectively. The overprediction generally does not exceed uncertainty limits but is indicative that a bias exists in the measurements or application of model. From this study, uncertainties in the particle number and mass size distributions as the cause for the model bias can be ruled out. The authors are also confident that the model is including the effects of growth kinetics on predicted activated number. However, one cannot rule out uncertainties associated with poorly characterized CCN measurement biases, uncertainties in assumed organic solubility, and uncertainties in aerosol mixing state. Sensitivity simulations suggest that assuming either an insoluble organic fraction or external aerosol mixing were both sufficient to reconcile the model bias.

** Current affiliation: Air Quality Research Division, Environment Canada, Toronto, Ontario, Canada.
++ Current affiliation: Centre for Ecology and Hydrology, Edinburgh, United Kingdom.
## Current affiliation: Scripps Institution of Oceanography, La Jolla, California.

*Corresponding author address:* Craig A. Stroud, 4905 Dufferin Street, Toronto, ON M3H 5T4, Canada.
E-mail: craig.stroud@ec.gc.ca

DOI: 10.1175/JAS3843.1

© 2007 American Meteorological Society

## 1. Introduction

Predictions for climate change vary, in large part, because of differences in the way the various feedback processes involving water vapor, aerosols, and clouds are represented in models (Nenes and Seinfeld 2003). Aerosols play a unique role in the earth's radiation budget by absorbing and scattering radiation (so-called direct aerosol effect) and influencing cloud optical properties (so-called indirect aerosol effect). Quantifying the impact of the indirect aerosol effect is a challenge because it requires that global models predict the aerosol size and composition as well as the interactions between gases, aerosols, water vapor, and clouds, most of which operate at the subgrid scale (Houghton et al. 2001).

The hygroscopic properties of aerosol particles are fundamental to their effectiveness as cloud condensation nuclei (CCN) (e.g., Charlson et al. 2001). An outstanding issue in cloud microphysics is achieving closure between predicted and observed CCN concentrations for the wide range of concentrations and chemical composition observed in ambient aerosol. Several studies have speculated that much of the variability of CCN is due to the variability of organic constituents in the ambient aerosol (Raymond and Pandis 2002; Mircea et al. 2002; O'Dowd et al. 2004; Rissman et al. 2004). Theory predicts that the activation of CCN depends strongly on their composition. Organic compounds can provide solute to the particle aqueous phase, affecting the water activity (Shulman et al. 1996; Laaksonen et al. 1998) and can directly affect particle surface tension (Facchini et al. 2000). Both of these effects alter the thermodynamic equilibrium of CCN with water vapor (so-called Köhler curve). Furthermore, surface-active organic compounds can form a film on the CCN and reduce the ability for water vapor to condense onto the CCN (Nenes et al. 2002; Feingold and Chuang 2002; Chuang 2003).

Aerosol activation is fundamental to understanding cloud formation because it influences the cloud droplet number concentration and, hence, cloud optical depth, precipitation, cloud lifetime, and albedo (e.g., Roberts et al. 2003). The water uptake of aerosol also impacts the number of cloud cycles in which a particle participates and largely controls its lifetime in the atmosphere. Aerosol-induced changes in cloud properties may feedback to surface evapotranspiration and thus the availability of water vapor in the atmosphere (Barth et al. 2005). Large-scale models must calculate the evolution of supersaturation, which is influenced by subgrid-scale temperature, water vapor, and vertical velocity. Large-scale models must also be able to represent the major properties of aerosol that affect the CCN spectrum in order to improve assessments of the indirect effect: the size distribution of the aerosol mass, the solubility of aerosol in water, and the amount of mixing of individual aerosol species within a given size fraction. Physically based parameterizations of cloud droplet formation for climate models (e.g., Nenes and Seinfeld 2003) do consider the aforementioned effects.

Mixed success has been met in prior studies that have attempted to compare modeled and measured CCN spectra (termed aerosol–CCN closure). In a significant number of prior closure studies, modeled CCN concentrations were larger than measured, although generally within uncertainty limits (Martin et al. 1994; Snider and Brenguier 2000; Chuang et al. 2000; Covert et al. 1998; Zhou et al. 2001; Cantrell et al. 2001; Snider et al. 2003; Dusek et al. 2003; Roberts et al. 2002; VanReken et al. 2003; Rissler et al. 2004). The positive model bias also increased for moderate to highly polluted conditions. Cantrell et al. (2001) found good general agreement between the measured and predicted CCN for marine aerosol sampled during the Indian Ocean Experiment (INDOEX) field program; however, the modeled CCN overpredicted observed CCN number concentration for one specific period when organic carbon was greater than 25% of total aerosol mass. VanReken et al. (2003) found that an idealized composition of pure $(NH_4)_2SO_4$ yielded good aerosol–CCN closure during the Cirrus Regional Study of Tropical Anvils and Cirrus Layers: Florida Area Cirrus Experiment (CRYSTAL FACE) for all flights with the exception of one. For this particular flight, CCN was elevated in concentration and back trajectories originated from the polluted boundary layer over Georgia several days earlier. The origin of the aerosol on this flight was not dissimilar to the location of the CELTIC field program.

Roberts et al. (2002) and Rissler et al. (2004) performed aerosol–CCN closures for aerosol sampled during the wet season over the Amazon. In this environment, aerosol mass composition is dominated by the organic fraction (80%) of which 50% is estimated to be water soluble organic compounds (WSOC). Inorganic salts are estimated to represent 15% of submicron aerosol mass. The large fraction of WSOC is believed to have originated from the oxidation of locally emitted biogenic gases and partitioning of semivolatile products to the aerosol phase. Roberts et al. (2002) predicted a similar contribution to CCN activity from the WSOC as that from the soluble inorganic component. However, large uncertainties where noted for the organic aerosol chemical speciation, solubility, and surface tension. Rissler et al. (2004) was also capable of achieving good aerosol–CCN closure for the wet season Amazon aero-

sol with CCN predictions generally within 25% of observations. They used hygroscopic tandem differential mobility analyzer (H-TDMA) measurements to characterize the WSOC fraction, insofar as the organic compounds go into solution at 90% relative humidity.

Snider et al. (2003) and Dusek et al. (2003) analyzed aerosol samples for CCN closure during the Aerosol Characterization Experiment (ACE-2) campaign. Snider et al. compared observations, for five study days, collected at a coastal site and on an aircraft over the eastern Atlantic Ocean. Measured and predicted CCN did agree after accounting for differences between the mobility equivalent and sphere equivalent diameters, but only when considering results from two study days unaffected by continental pollution. Dusek et al. (2003) analyzed data collected in southern Portugal and showed that WSOC constitutes less than 10% of the total aerosol mass. In recognition of this, Dusek et al. ignored contributions of the organic carbon to CCN activity. Calculated CCN were overestimated by, on average, 30%, which they state is comparable to the uncertainties in their measurements and predictions.

After reviewing the results of prior studies, one common hypothesis emerges to explain the model overpredictions. The discrepancy has generally been attributed to an incomplete understanding of the aerosol composition, especially the role of organic species in the activation process. Field programs where the aerosol is largely composed of soluble material (marine and Amazon studies) have achieved better agreement than studies where aerosol is influenced by continental pollution sources.

The goal of this study was to measure the mass size distribution of the organic and inorganic aerosol components for the size range critical to CCN activation (around 100 nm diameter) coincident with measurements of aerosol number size distribution and CCN number and subsequently evaluate whether the measurements of size-resolved organic aerosol can improve our ability to predict CCN number compared to prior closure studies. Measurements were acquired in the summertime over North Carolina during the Chemical Emission, Loss, Transformation, and Interactions within Canopies (CELTIC) field program. The aerosol sampled was impacted by a combination of biogenic and anthropogenic sources and, thus, provided a stringent test of cloud activation theory.

## 2. Experimental design

### *a. Site description*

CELTIC took place at the Duke Forest C-H2O Research Site in North Carolina (35.98°N, 79.09°W) in collaboration with the U. S. Department of Energy (Office of Biological and Environmental Research and National Institute for Global Environmental Change) and Department of Agriculture (Southern Global Change Program) sponsored the Forest–Atmosphere Carbon Transfer and Storage (FACT; FACTS-1, operated by the Brookhaven National Laboratory) and AmeriFlux studies. Duke Forest is a loblolly pine plantation with approximate tree heights of 18 m. The site consists of six free-air $CO_2$ enrichment (FACE) rings, three of which provide elevated atmospheric $CO_2$ concentrations, and three are ambient control rings. Aerosol measurements were performed at control ring 6 on a 26-m tower. The plantation is approximately 330 m $\times$ 800 m in area with ring 6 having a fetch of approximately 400 m for predominant wind directions from the southwest. Duke Forest is located between the towns of Chapel Hill (10 km to SSE), Durham (20 km to ENE), Raleigh (40 km to SE), and Burlington (30 km to WNW). The closest major highway is Interstate 40 (2.4 km to the NE).

### *b. Measurement description*

CCN spectra were recorded with a University of Wyoming thermal-gradient static-diffusion cloud chamber (CCNC-100A) (Snider and Brenguier 2000; Delene and Deshler 2000; Snider et al. 2003). The CCN instrument optically counted the number concentration of aerosol activated to cloud drop sizes. The CCN counter was calibrated by introducing NaCl aerosol of known number concentration and monodisperse distribution (greater than critical diameter) into the chamber at a given supersaturation and measuring the peak detector voltage difference between flush and detect cycles. The CCN counter was stepped over a supersaturation range generating a CCN concentration per voltage difference versus supersaturation relationship, which was then used in subsequent measurements. For a given supersaturation, measured voltage differences were converted to CCN concentrations. Nominal supersaturation calculated from chamber theory and recorded by the data acquisition system were multiplied by a correction factor ($S_{\text{nominal}}/S_{\text{effective}} = 0.65$) to generate effective supersaturation, as discussed in Snider et al. (2003). This correction factor accounts for uncertainties associated with differences between pad and thermocouple temperature and differences between pad water-vapor equilibrium and pure water vapor equilibrium. The CCN counter was physically mounted 23 m above ground on the tower. The CCN counter was operated between 0.13% and 0.33% supersaturation. Figure 1 illustrates the CCN time series concentrations as a function of cloud chamber supersaturation. For extreme

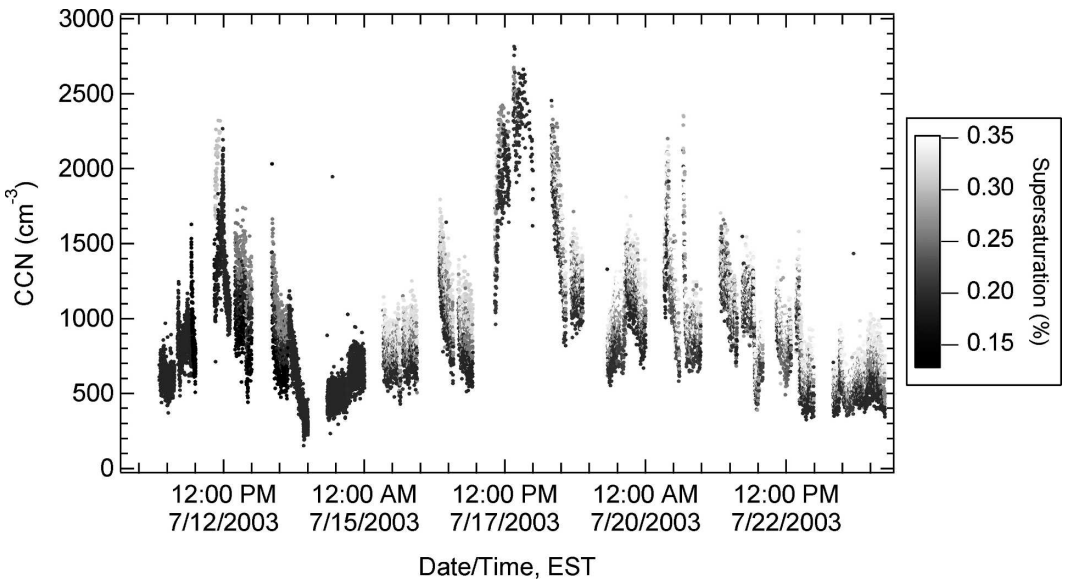


FIG. 1. Observed CCN number concentration time series color-coded as a function of percentage supersaturation. EST is eastern standard time.

pollution events, the CCN detector voltage went off-scale at higher supersaturation, and thus CCN concentrations were not obtained (CCN number concentration $>2800$ cm$^{-3}$).

Aerosol size distributions were recorded with two separate scanning mobility particle sizer instruments (TSI, SMPS Model 3936). The nano-SMPS was operated in a mobility diameter ($d_m$) range of 5–60 nm while the long SMPS was operated in a $d_m$ range of 20–600 nm. The size distributions from each instrument were compared to each other and to the total number concentration from two condensation particle counter (TSI, CPC Models 3025 and 3022). The nano-SMPS typically recorded number concentrations a factor of 1.38 higher than the long SMPS for overlapping sizes. In comparing the summed number concentration over all size bins, the long SMPS achieved good closure with the TSI 3022 (TSI 3022 being only a few percent higher than long SMPS). On average, the TSI 3025 was a factor of 1.10 higher than the TSI 3022, likely reflecting the number of particles between the lower particle diameter limits of each instrument. As a result of these comparisons, we have confidence in the quality of the long-SMPS measurements. The nano-SMPS number concentrations were divided by 1.38 for creating a merged particle size distribution (see Fig. 4). The nano-SMPS data was not used in the aerosol–CCN closure to follow, as the particle sizes that are uniquely measured by this instrument are too small to activate with the supersaturations used here. The SMPS instruments were situated in a trailer and sampled air from a manifold, which drew air down a 30-m copper line (1/2″ O.D.) at a flow rate of 11.5 L min$^{-1}$ from above the canopy. Delia (2004) estimated upper limit line losses of 12% for submicron particle transmission in the sampling system.

Two Aerodyne aerosol mass spectrometers (AMS) (Jayne et al. 2000; Jimenez et al. 2003) were also situated in the trailer and sampled air from the manifold. One AMS was primarily used for particle flux measurements [termed Cooperative Institute for Research in Environmental Sciences (CIRES) AMS], while the other was used for a continuous time series of aerosol composition and size distributions versus $d_{va}$ [Delia (2004), termed Program for the Atmospheric and Oceanic Sciences (PAOS) AMS]. The two AMS instruments compared well with each other with the exception of ammonium mass concentration. The PAOS AMS instrument typically measured higher ammonium mass concentrations by a factor of 2. Given the unrealistically large ammonium mass concentrations compared to the other anionic aerosol components (e.g., case 1 had ammonium, nitrate, and sulfate mass concentrations of 4.2, 0.42, and 4.2 $\mu$g m$^{-3}$, respectively), the PAOS AMS ammonium mass concentrations were halved in the CCN closure study to follow.

### c. CCN closure study

Four periods of approximately two-hour duration each were chosen for the CCN closure studies. Periods were chosen to meet three criteria: 1) uniform CCN concentration throughout a given sampling period, 2) differing levels of pollution between sampling periods,

and 3) adequate data coverage from the CCN, SMPS, and PAOS AMS during the sampling period. For each case, data were averaged over the sampling period to create a representative CCN supersaturation spectra, aerosol number size distribution, and composition-resolved mass size distribution.

A fitting algorithm based on the theoretical relationships between the particle properties and the mobility and vacuum aerodynamic equivalent diameters (DeCarlo et al. 2004) was used to integrate measurements from the SMPS (number and apparent volume distributions) and PAOS AMS instrument (mass concentrations versus vacuum aerodynamic diameter for sulfate, nitrate, ammonium, and organics) into a single, coherent description of the ambient aerosol (DeCarlo et al. 2005, unpublished manuscript). First, the SMPS mobility particle diameters were converted to volume-equivalent diameters ($d_{ve}$) using

$$d_m/C_c(d_m) = \chi_t d_{ve}/C_c(d_{ve}), \quad (1)$$

where $\chi_t$ is the dynamic shape factor in the transition regime relevant for the SMPS and $C_c$ is the Cunningham slip correction factor (function of $d_{ve}$ or $d_m$). Second, the AMS vacuum aerodynamic diameters were converted to volume-equivalent diameters:

$$d_{ve} = d_{va}\chi_v(\rho_0/\rho_p), \quad (2)$$

where $\chi_v$ is the dynamic shape factor in the free molecular regime relevant to the AMS, $\rho_p$ is the particle density, and $\rho_0$ is the standard density (1 g cm$^{-3}$). Observations were then fit into three lognormal modes with parameters for number, geometric mean diameter, geometric standard deviation, shape factor, and percent composition for sulfate, nitrate, ammonium, and organics. Table 1 lists the parameters derived from the fitting algorithm for each case. As the AMS does not measure elemental carbon, we assumed an ORG:EC ratio of 4:1 for modes 1 and 2 (Turpin and Lim 2001; Cabada et al. 2004) where ORG is the organic mass (including carbon and other atoms) and EC is the elemental carbon mass. Mode 3 did not include elemental carbon. The composition of mode 1 was also held constant and estimated based on the composition of Aitken mode primary combustion aerosol. The composition of modes 2 and 3 and the number and median diameter of all three modes were iterated in the fitting algorithm. The fitting algorithm also assumed that each mode had a constant shape factor (and with $\chi_t = \chi_v$) and a constant AMS collection efficiency versus size. Each mode also had a unique composition different from that of the other two modes; however, within a mode the composition was internally mixed over the size distribution.

A cloud chamber kinetic model was used to perform the aerosol–CCN closure study for each case (Nenes et al. 2001). The kinetic model first calculated the supersaturation field within the chamber and then simulated the growth of the CCN as they activate. Condensational growth and gravitational settling are considered over the 20-s measurement cycle. The kinetic model included a modified Köhler theory to calculate surface water vapor pressures for the three composition-resolved size modes, as well as a size-dependent, mass transfer limited treatment of water vapor condensation. The kinetic model inputs for all three lognormal modes included: 1) total number $N_{tot}$, geometric standard deviation, $\sigma_g$, and geometric mean diameter $d$; 2) salt composition, density, and mass fraction; 3) organic composition, density, mass fraction, and solubility; 4) insoluble mass fraction and density; and 5) water vapor accommodation coefficient.

After running the SMPS–AMS fitting routine, we derived representative inorganic salt compositions for input into the CCN model, constrained by mass conservation. First, aerosol nitrate was assumed to form $NH_4NO_3$. The remaining ammonium was assumed to bond with sulfate as either $(NH_4)_2SO_4$, $(NH_4)_2SO_4$ and $(NH_4)_3H(SO_4)_2$, $(NH_4)_3H(SO_4)_2$ and $NH_4HSO_4$, or $NH_4HSO_4$. The form depended on the $NH_4/SO_4$ molar ratio. It is noted that, assuming the nitrate in the form of $NH_4NO_3$, may not yield a thermodynamically stable state. An organic aerosol composition of levoglucosan (15% by mass), pinic acid (41% by mass), and fulvic acid (41% by mass) was assumed to calculate representative organic density, organic Van't Hoff factor and organic molecular weight (Nenes et al. 2002). Table 2 lists the pure component physical properties for these surrogate organic species. From the soluble inorganic salt fraction, partially soluble organic fraction and insoluble elemental carbon fraction, mass-weighted average particle density, Van't Hoff factor, and molecular weight were calculated for each mode (Table 1).

A critical issue in reconciling the simulations with the observations is the activation time scale within the static thermal gradient cloud chamber. During the activation period, particles take a finite period of time to grow to a certain size before they fall out of the view volume, resulting in a peak in detector voltage. The time scale for particle growth depends on instrument supersaturation, particle size, and growth kinetics. Complex growth kinetics can arise from numerous mechanisms: 1) multicomponent partially soluble organics, which cause multiple cusps on a Köhler curve (Shulman et al. 1996; Shantz et al. 2003); 2) from an organic film, which can potentially decrease the water vapor accommodation coefficient; and 3) finite dissolution kinetics (Asa-Awuku and Nenes 2007). The aero-

TABLE 1. Aerosol chemical and physical properties for selected case studies.

| Aerosol property | Case 1 0930–1130 EST 16 July | Case 2 1030–1330 EST 17 July | Case 3 2030–2300 EST 17 July | Case 4 1745–2000 EST 18 July |
|---|---|---|---|---|
| Mode 1 | | | | |
| Mass fraction organic | 0.77 | 0.77 | 0.77 | 0.77 |
| Mass fraction elemental carbon | 0.16 | 0.16 | 0.16 | 0.16 |
| Mass fraction $(NH_4)_2SO_4$ | 0.040 | 0.040 | 0.040 | 0.040 |
| Mass fraction letovicite | 0 | 0 | 0 | 0 |
| Mass fraction $NH_4HSO_4$ | 0 | 0 | 0 | 0 |
| Mass fraction $NH_4NO_3$ | 0.027 | 0.027 | 0.027 | 0.027 |
| Soluble density (kg $m^{-3}$) | 1748 | 1748 | 1748 | 1748 |
| Soluble Van't Hoff | 2.2 | 2.2 | 2.2 | 2.2 |
| Soluble molecular weight (kg $mol^{-1}$) | 0.104 | 0.104 | 0.104 | 0.104 |
| Soluble mass fraction | 0.067 | 0.067 | 0.067 | 0.067 |
| Partially soluble density (kg $m^{-3}$) | 1130 | 1130 | 1130 | 1130 |
| Partially soluble Van't Hoff | 2.7 | 2.7 | 2.7 | 2.7 |
| Partial soluble molecular weight (kg $mol^{-1}$) | 0.26 | 0.26 | 0.26 | 0.26 |
| Partially soluble mass fraction | 0.77 | 0.77 | 0.77 | 0.77 |
| Insoluble density (kg $m^{-3}$) | 2250 | 2250 | 2250 | 2250 |
| Insoluble mass fraction | 0.16 | 0.16 | 0.16 | 0.16 |
| Number concentration ($cm^{-3}$) | 711 | 1500 | 600 | 300 |
| Median diameter (nm) | 31 | 35 | 60 | 35 |
| Geometric standard deviation | 1.56 | 1.56 | 1.56 | 1.56 |
| Dynamic shape factor | 1.0 | 1.0 | 1.0 | 1.0 |
| Mode 2 | | | | |
| Mass fraction organic | 0.72 | 0.58 | 0.62 | 0.69 |
| Mass fraction elemental carbon | 0.15 | 0.12 | 0.13 | 0.14 |
| Mass fraction $(NH_4)_2SO_4$ | 0.098 | 0.087 | 0 | 0 |
| Mass fraction letovicite | 0 | 0.18 | 0.043 | 0 |
| Mass fraction $NH_4HSO_4$ | 0 | 0 | 0.17 | 0.12 |
| Mass fraction $NH_4NO_3$ | 0.033 | 0.043 | 0.039 | 0.052 |
| Soluble density (kg $m^{-3}$) | 1755 | 1769 | 1777 | 1767 |
| Soluble Van't Hoff | 2.3 | 3.3 | 2.6 | 2.3 |
| Soluble molecular weight (kg $mol^{-1}$) | 0.133 | 0.159 | 0.117 | 0.101 |
| Soluble mass fraction | 0.13 | 0.31 | 0.25 | 0.17 |
| Partially soluble density (kg $m^{-3}$) | 1130 | 1130 | 1130 | 1130 |
| Partially soluble Van't Hoff | 2.7 | 2.7 | 2.7 | 2.7 |
| Partial soluble molecular weight (kg $mol^{-1}$) | 0.258 | 0.258 | 0.258 | 0.258 |
| Partially soluble mass fraction | 0.72 | 0.58 | 0.62 | 0.69 |
| Insoluble density (kg $m^{-3}$) | 2250 | 2250 | 2250 | 2250 |
| Insoluble mass fraction | 0.15 | 0.12 | 0.13 | 0.14 |
| Number concentration ($cm^{-3}$) | 2646 | 5639 | 4994 | 2652 |
| Median diameter (nm) | 125 | 121 | 147 | 130 |
| Geometric standard deviation | 1.72 | 1.41 | 1.34 | 1.68 |
| Dynamic shape factor | 1.0 | 1.15 | 1.10 | 1.14 |
| Mode 3 | | | | |
| Mass fraction organic | 0.24 | 0.40 | 0.55 | 0.45 |
| Mass fraction elemental carbon | 0 | 0 | 0 | 0 |
| Mass fraction $(NH_4)_2SO_4$ | 0.72 | 0 | 0 | 0.44 |
| Mass fraction letovicite | 0 | 0 | 0.032 | 0 |
| Mass fraction $NH_4HSO_4$ | 0 | 0.55 | 0.38 | 0 |
| Mass fraction $NH_4NO_3$ | 0.034 | 0.046 | 0.040 | 0.11 |
| Soluble density (kg $m^{-3}$) | 1766 | 1783 | 1783 | 1758 |
| Soluble Van't Hoff | 2.5 | 2.4 | 2.5 | 2.4 |
| Soluble molecular weight (kg $mol^{-1}$) | 0.128 | 0.111 | 0.115 | 0.117 |
| Soluble mass fraction | 0.76 | 0.60 | 0.45 | 0.548 |
| Partially soluble density (kg $m^{-3}$) | 1130 | 1130 | 1130 | 1130 |
| Partially soluble Van't Hoff | 2.7 | 2.7 | 2.7 | 2.7 |
| Partial soluble molecular weight (kg $mol^{-1}$) | 0.258 | 0.258 | 0.258 | 0.258 |

TABLE 1. (*Continued*)

| Aerosol property | Case 1 0930–1130 EST 16 July | Case 2 1030–1330 EST 17 July | Case 3 2030–2300 EST 17 July | Case 4 1745–2000 EST 18 July |
|---|---|---|---|---|
| Mode 3 | | | | |
| Partially soluble mass fraction | 0.24 | 0.40 | 0.55 | 0.45 |
| Insoluble density (kg $m^{-3}$) | 2250 | 2250 | 2250 | 2250 |
| Insoluble mass fraction | 0 | 0 | 0 | 0 |
| Number concentration ($cm^{-3}$) | 667 | 1002 | 1306 | 559 |
| Median diameter (nm) | 285 | 215 | 244 | 326 |
| Geometric standard deviation | 1.43 | 1.58 | 1.44 | 1.36 |
| Dynamic shape factor | 1.07 | 1.10 | 1.12 | 1.14 |

sol population will have a distribution of residence times for growth to scattering sizes within the viewing volume. The heterogeneity in the aerosol composition leads to shifts in the peak voltage intensity and time.

This study used the initial increase of the CCN instrument voltage to help constrain an estimate for the water vapor accommodation coefficient, $\alpha$. We averaged the CCN voltages over all activations within the approximate 2-h sampling periods. Figure 2 presents the initial growth curves for the four case study periods. Figure 2 also presents the modeled growth curves for a constant $\alpha = 0.07$ across all three modes. We decided to focus on the initial 5 s of the growth period, similar to the time period analyzed by Shantz et al. (2003) within the same instrument design. We decided to focus on the initial growth in estimating $\alpha$ because other competing processes such as coagulation and droplet fallout are of lesser importance and, thus, the system is more constrained. In our estimation of $\alpha$, we do not consider the model—measurement differences due to the fact that the model predicts number concentration and the observations are of scattering voltage. We did not perform concurrent video camera measurements of CCN number within the instrument chamber, as performed by Delene and Deshler (2000). Therefore, we rely on the results from Delene and Deshler to estimate the magnitude of this effect. From Figs. 4 and 5 in Delene and Deshler (2000), the peak voltage appears to lag the peak number by approximately 2 s for $S = 0.3\%$. We performed an additional sensitivity run for case 3, shown in Fig. 3, where we varied the $\alpha$ between 0.04 and 0.10. The modeled number maximum is shifted to shorter times with increases in $\alpha$. Owing to the lack of direct measurements for the lag between voltage and number, we do not attempt to account for these differences in our best-fit estimation of $\alpha$. As a result, our inferred $\alpha$ value is considered a lower limit; however, we feel that the uncertainty added to $\alpha$ due to the time lag between voltage and number will be small. Evidence to support this comes from Fig. 3 where a small variation in $\alpha$ (from 0.07 to 0.10) is predicted to shorten the time to reach maximum by 4 s. A wide range of $\alpha$ values have been reported in the literature. Lance et al. (2004, hereafter L04) assumed $\alpha = 0.042$ for their cloud parcel model simulations. As noted in L04, $\alpha = 0.042$ is typical of $H_2O$ accommodation coefficients used in earlier cloud modeling studies (Pruppacher and Klett 2000) for inorganic aerosol. More recent aerosol–cloud droplet closure studies, as summarized in Table 7 of McFiggans et al. (2006), show a range of $\alpha$ from 0.04 to 1.00. Even more recently, Meskhidze et al. (2005) and Fountoukis et al. (2007) conducted aerosol–cloud droplet closure using in situ observations of cumuliform and stratiform clouds formed in polluted and clean air masses; both studies achieved best closure for $\alpha$ ranging between 0.03 and 0.06. Our estimate of $\alpha = 0.07$ lies very close to all of these estimates. Chuang (2003) summarizes the body of literature on the time scale of hygroscopic growth for ambient aerosol. Chuang (2003) measured condensation growth time scales for aerosol with diameters of 50–100 nm in Mexico City. Most particles that they observed exhibited growth time scales corresponding to $\alpha$ of order $10^{-2}$ to $10^{-4}$; however a small fraction of particles (0%–2%) exhibited longer time scales corresponding to $\alpha$ as low as $10^{-5}$. It is also well established from laboratory experiments that the presence of an organic film on a flat liquid surface is able to limit $\alpha$ across the liquid–gas interface. Laboratory studies on synthetic aerosol composed of organic films do suggest that $\alpha$ on the order of $10^{-4}$ to $10^{-5}$ are possible (Otani and Wang 1984; Rubel and Gentry 1984; Seaver et al. 1992). As noted in McFiggans et al. (2006), surfactant films on ambient aerosol are more likely to be expanded and porous, rather than con-

TABLE 2. Physical properties of organic aerosol surrogates.

| Surrogate | Molecular weight (g $mol^{-1}$) | Van't Hoff factor | Density (kg $m^{-3}$) |
|---|---|---|---|
| Pinic acid | 186 | 3 | 800 |
| Fulvic acid | 732 | 5 | 1500 |
| Levoglucosan | 162 | 1 | 1600 |

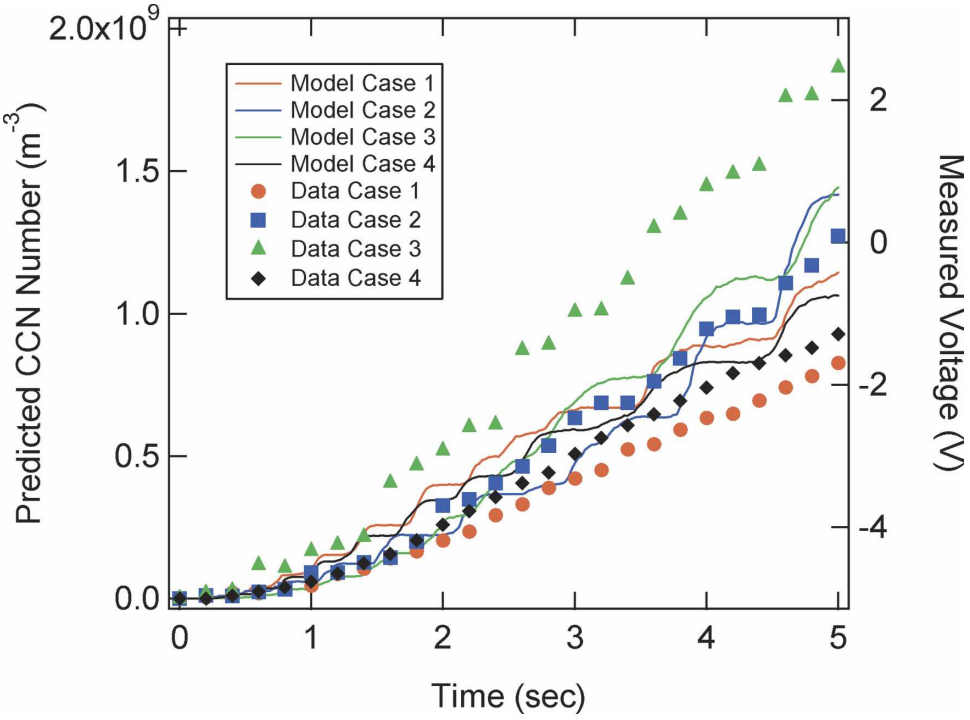


FIG. 2. Measured scattering voltage recorded by the CCN counter during the first 5 s of activation period averaged for each of the four case studies. An offset voltage was added to each trace so that all four cases started at −5 V. Also included are model-derived CCN number concentrations along the centerline of the CCN chamber.

densed and ordered, and are likely to play a lesser role in limiting water-vapor mass transfer compared to laboratory synthetic aerosol.

An important issue in interpreting the model output is defining the size of the smallest detectable activated droplet. Here, we assume that aerosol with diameters greater than 2.5 $\mu$m are activated and, thus, are CCN. This cutoff removes interferences from interstitial (or haze) aerosol in the diameter range 1–2.5 $\mu$m (e.g., dust, pollen), which does not contribute to cloud droplet number and, hence, CCN. However, this cutoff can also impact activated particles with slow growth kinetics. Simulations performed at $S = 0.2\%$ were sensitive to the lower diameter cutoff (1 or 2.5 $\mu$m) for counting CCN.

The organic fraction was assumed to have a base case solubility of 0.02 kg kg$^{-1}$ (L04). For comparison, pinic acid, norpinic acid, adipic acid, and leucine have pure water solubilities of 0.085, 0.047, 0.018, and 0.009 kg kg$^{-1}$, respectively. Nenes et al. (2002) showed that CCN characteristics for both marine and urban aerosol are sensitive to organic solubilities between $10^{-2}$ and $10^{-3}$ kg kg$^{-1}$. We performed a sensitivity simulation for all cases with insoluble organic fraction to assess the upper-limit impact of uncertainties in organic solubility.

## 3. Results

### a. Time series trends

Figure 4 presents the time series trends for aerosol microphysical and chemical measurements. Figure 4a

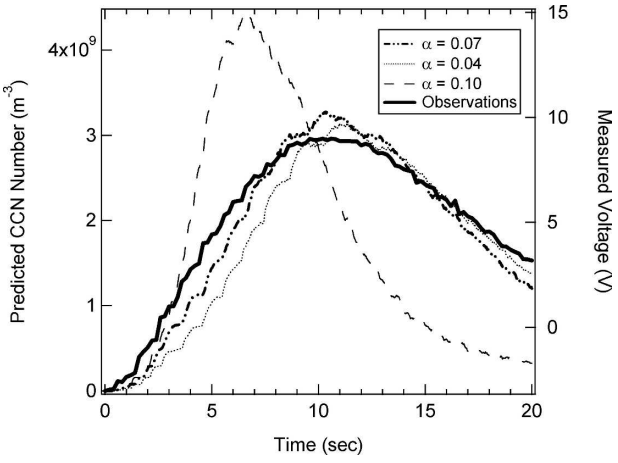


FIG. 3. Measured scattering voltage recorded by the CCN counter during the 20-s activation period for case 3 (solid line). Also included are model-derived CCN number concentrations for varying water-vapor accommodation coefficients between 0.04 and 1.0 (dashed lines).

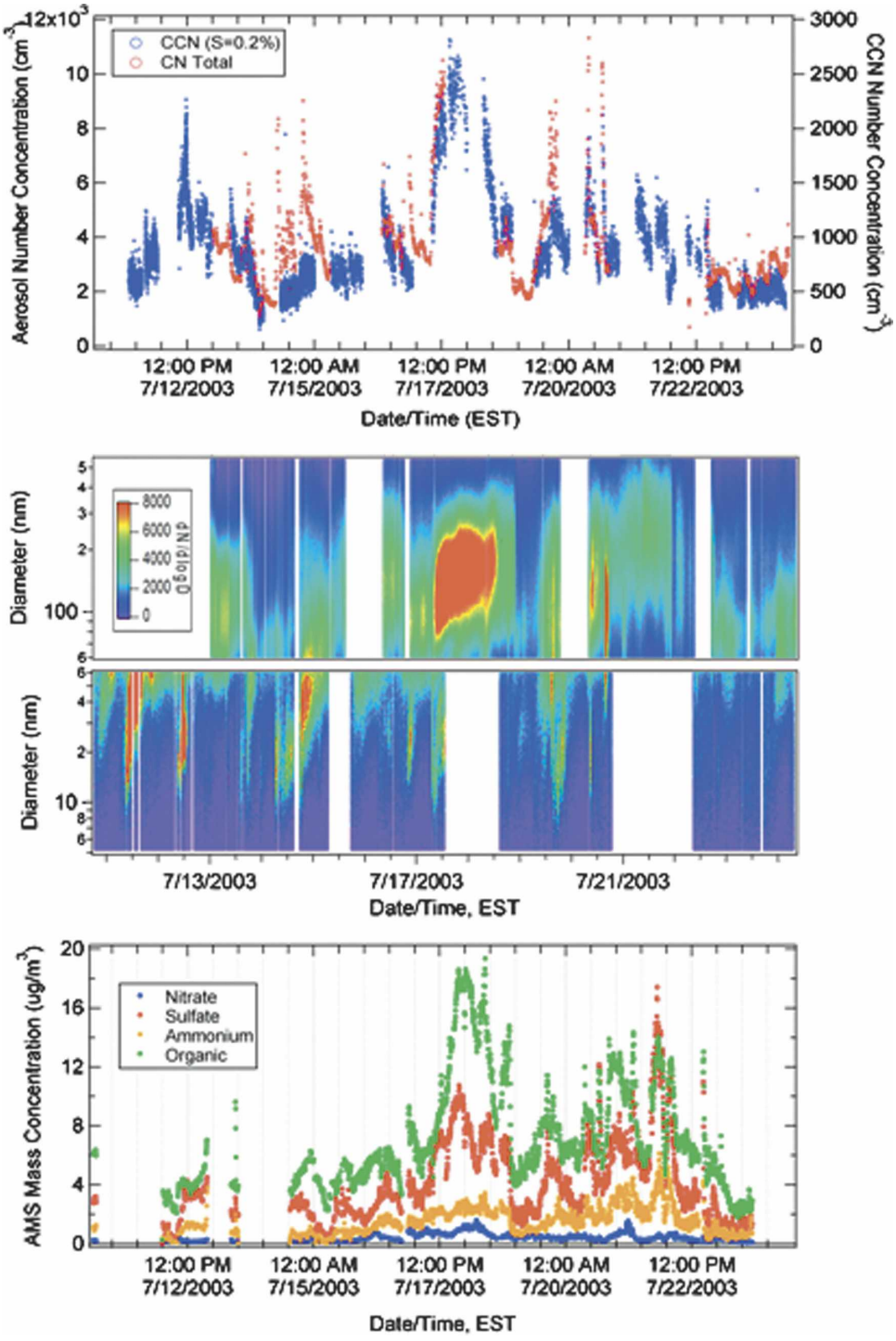


FIG. 4. Observed time series for (a) total aerosol number concentration and CCN number concentration ($S$ = 0.2%), (b) aerosol size distribution, and (c) aerosol component mass concentrations.

illustrates the SMPS aerosol number concentration (nano-SMPS from $d_m$ = 5–20 nm plus long SMPS from $d_m$ = 20–600 nm) time series. For the entire field program, the maximum and minimum aerosol number concentration was 694 and 11 325 cm$^{-3}$, respectively with a median value of 3414 cm$^{-3}$. Generally, maxima in the aerosol number concentration time series occurred in the morning (0700–0930 EST) and evening (1500–1800

EST), likely associated with local traffic emissions and changes in air mass associated with vertical mixing. One pronounced period of prolonged pollution was observed from 0700 EST 17 July 2003 and lasting until the afternoon of 18 July 2003. Figure 4a also includes the CCN number concentration ($S = 0.2\%$) observations. The maximum and minimum CCN number concentrations ($S = 0.2\%$) for the entire field program were 2815 and 153 $cm^{-3}$ with a median value of 707 $cm^{-3}$. Considering these median values, 21% of the SMPS aerosol number acted as CCN at $S = 0.2\%$. The 2-day pollution episode was also observed in the CCN observations with a strong correlation between SMPS aerosol number and observed CCN number.

Figure 4b illustrates the SMPS number size distribution time series. The striking feature is the large $dN/d\log d_m$ values in the accumulation mode ($d_m$ = 100–300 nm) during the 2-day pollution episode starting 0700 EST 17 July 2003. Other shorter duration periods with significant accumulation mode number concentrations were 0820–1000 EST 20 July 2003 and 1519–1634 EST 20 July 2003. These periods also exhibited maxima in CCN number concentration. Figure 4b also shows periods with large Aitken mode number concentrations ($d_m$ = 10–30 nm) such as at 2000–2100 EST 16 July 2003 and 0624–0724 EST 14 July 2003. Coincident local maxima were observed for no mixing ratios, suggesting that the large Aitken mode number concentrations for these periods were due to local traffic emissions. These periods did not show up as maxima in CCN concentration as the Aitken mode size range is too small to activate to cloud drops within the CCN instrument for the $S = 0.2\%$–$0.33\%$ range. Figure 4b also illustrates a significant growth event starting from the Aitken mode at 1739 EST 14 July 2003. Aerosol growth occurred until 2359 EST 14 July 2003 with particle diameters increasing to approximately 70 nm. Again, no significant increases in CCN number concentration occurred during this growth event.

Figure 4c presents the AMS time series observations for aerosol organic (ORG), $SO_4$, $NO_3$, and $NH_4$ mass concentrations between $d_{va}$ = 100 and 600 nm. Most of the time, the organic mass concentration was larger than sulfate. The nitrate mass concentration was always much less than the sulfate and, thus, contributes a small amount of solute for the CCN. The 2-day pollution event discussed earlier can also be seen in the AMS composition data. Interestingly, the sulfate mass fraction increased at 0700 EST 17 July 2003 coincident with aerosol number concentration. However, the organic aerosol component lagged in time with its increase. Maximum sulfate and organic mass concentrations occurred at 2120 EST 17 July 2003 and 0100 EST 18 July 2003. Both of these maxima in mass concentration were considerably delayed from the maximum in aerosol number concentration (1229 EST 17 July 2003). The reader is referred to Delia (2004) for a more complete description of the AMS measurements during CELTIC.

### b. Case studies

A series of case studies were chosen to evaluate aerosol–CCN closure (Table 1). The first and fourth cases were chosen before and after the 2-day pollution episode and represent average aerosol conditions observed at Duke Forest during the CELTIC study. The second case represents the early stages of the pollution episode with a large $SO_4$/ORG aerosol mass concentration ratio. The third case represents the later stages of the pollution episode with a more typical $SO_4$/ORG aerosol mass concentration ratio. Figure 5 presents the 72-h isentropic back trajectories for each case generated using the NOAA Hybrid Single-Particle Lagrangian Integrated Trajectory (HYSPLIT) Air Resource Laboratory Web site (http://www.arl.noaa.gov/ready/hysplit4.html). Back trajectory analysis indicates a change in air mass origin aloft of the site throughout night of 17 July 2003 with winds shifting from the southwest to the northeast direction. The polluted air mass aloft then convectively mixed down to the site during the morning on 17 July 2003. Back trajectories from the first and fourth cases originated from the southwest, which is the prominent summertime wind direction at Duke Forest. Back trajectories from the second and third cases during the pollution episode originated from the northeast in the direction of Raleigh and the Ohio River Valley. These back trajectories are consistent with local changes in wind direction observed at the site.

Whether or not the CCN measurements are influenced by anthropogenic emissions can be assessed from observations of $O_3$ and $NO_x$. Figure 6 illustrates ancillary measurements of $O_3$, $NO_x$ (sum of NO and $NO_2$) during the case study periods. The $O_3$ and $NO_x$ mixing ratios were in the range 55–58 and 0.5–1 ppbv during the afternoon on both 16 and 18 July 2003. During the pollution episode, $O_3$ and $NO_x$ mixing ratios on the afternoon of 17 July 2003 were 70 and 1.2–1.7 ppbv, respectively. Isoprene dominated hydrocarbon reactivity at the forested site. Typical midday isoprene and monoterpene mixing ratios were 1.6 and 0.4 ppbv, respectively (Stroud et al. 2005). Isoprene peaked in mixing ratio in the evening with an average maximum of 2.7 ppbv. Monoterpenes peaked in mixing ratio during the night, typically at 1.7 ppbv.

Relative humidity can be used qualitatively as an in-

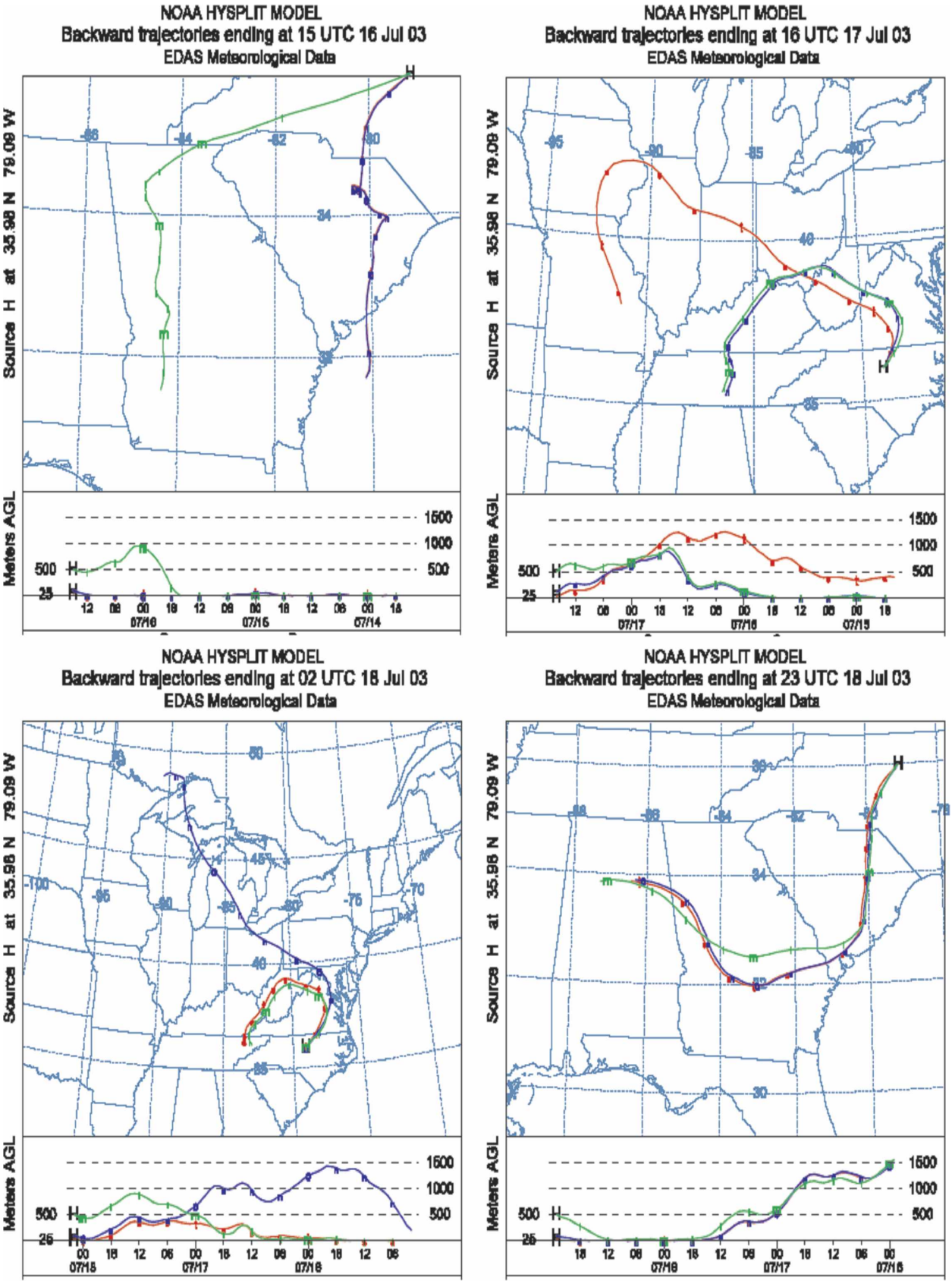


FIG. 5. Back trajectories calculated for the four selected case studies using the NOAA Air Resources Laboratory HYSPLIT program (case 1: upper left, case 2: upper right, case 3: lower left, case 4: lower right).

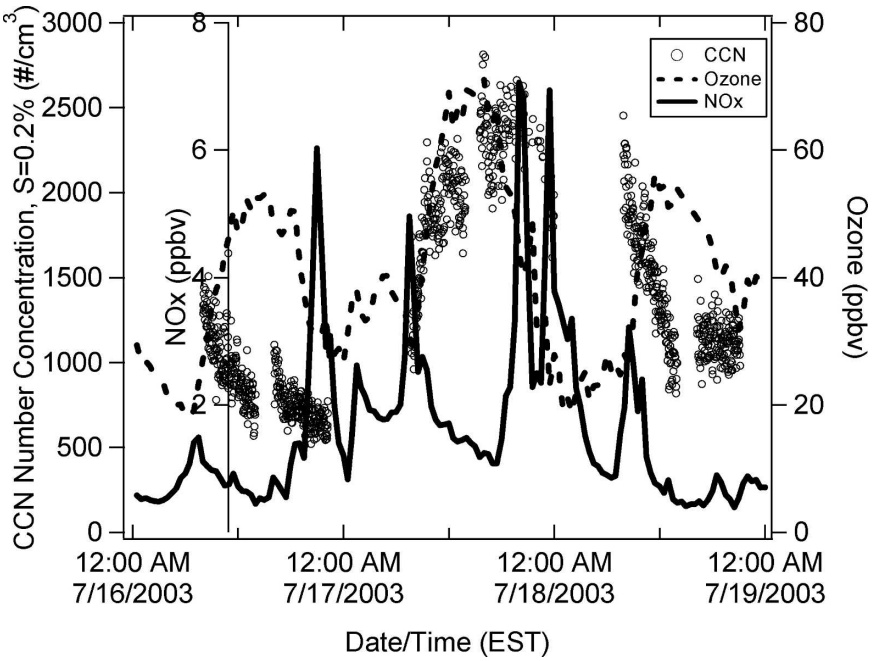


FIG. 6. Observed time series for $O_3$ mixing ratio, $NO_x$ mixing ratio, and CCN number concentration ($S = 0.2\%$).

dicator of the growth of the surface mixing layer in the morning (Stroud et al. 2002). On the morning of 0715 EST 17 July 2003, the relative humidity abruptly decreased with the mixing of drier air aloft to the site (Fig. 7). At the same time, $O_3$ and CCN increased as the polluted air mass aloft was mixed down to the surface (Fig. 6). This is in contrast to 16 and 18 July 2003, when lower CCN concentrations were observed in the regional air mass above the site and resulted in a decreasing time series trend with the onset of vertical mixing in the morning.

Figures 8 and 9 present size distributions derived from the SMPS and chemical composition obtained from the AMS for the first and second case study periods, respectively. Panels in Figs. 8 and 9 are included for $dN/d \log d_m$, $dV/d \log d_m$, and $dM/d \log d_{va}$ for each chemical component. The thick colored lines in each panel represent the measured distributions and should be compared to the thin red lines, which are the summation of the three individual fitted spectra (orange lines for smallest size mode, blue lines for intermediate size mode, and green lines for largest size mode). Reasonable fits were also derived for the remaining two case studies (not shown here). Organics dominated the mass of modes 1 and 2 (mass fraction between 0.58 and 0.77). Sulfate was the second largest component in the form of ammonium sulfate for cases 1 and 4, and as ammonium bisulfate and letovicite for cases 2 and 3. Minor contributions were observed for the elemental carbon and nitrate fractions (see Table 1 for summary of size-resolved aerosol composition data). The composition of mode 2, which is critical in determining CCN concentration, resulted in this mode having a water solubility largely impacted by the water solubility of the organic fraction. The composition of mode 3 was primarily dominated by the inorganic ions, 45%–76% by mass, a mixture of ammonium, sulfate, and nitrate. As for modes 1 and 2, the nitrate was a small fraction of the inorganic mass. The organic fraction was the second largest fraction for mode 3 with a mass fraction between 0.24 and 0.55.

### BASE CASE SIMULATIONS

The CCN model was initialized with the chamber dimensions, sidewall thickness, wall conductivity, inlet line pressure, temperature, relative humidity, bottom and upper plate temperatures, and inlet aerosol properties. A computational grid of 100 cells in the radial and 100 cells in the axial direction was used for the simulations. Figure 10 illustrates the collective results for the aerosol–CCN closure by plotting the predicted versus observed CCN concentrations. Individual points are coded by shape representing supersaturation (circles for $S = 0.2\%$, squares for $S = 0.27\%$, and triangles for $S = 0.33\%$) and contrast representing sensitivity run conditions (dark points represent ORG solubility of 0.02 kg $kg^{-1}$ and light points represent ORG insoluble). Table 3 summarizes the results of the clo-

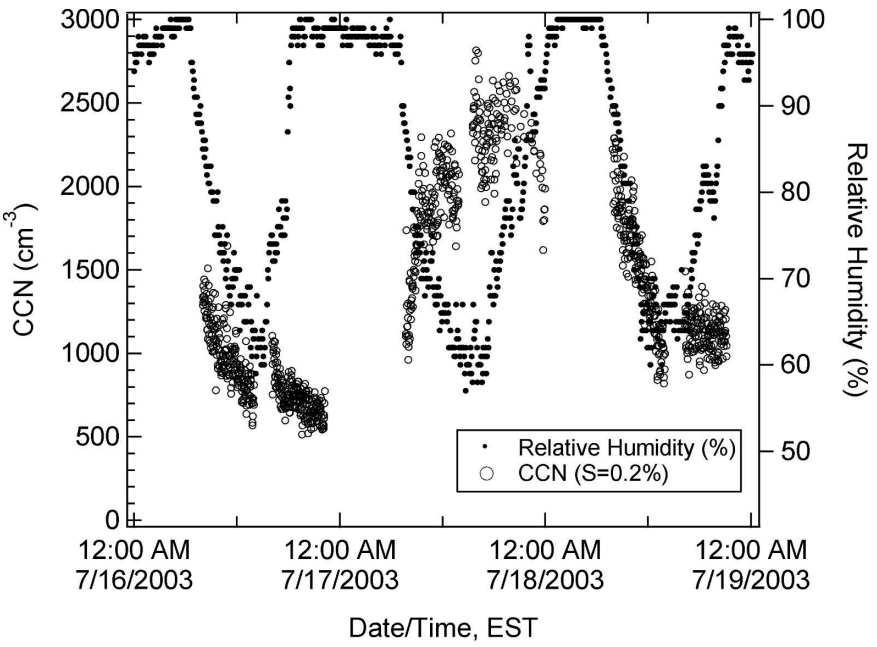


FIG. 7. Observed time series for relative humidity and CCN number concentration ($S = 0.2\%$).

sure study. The regression slope in Fig. 10 for the base case is 1.9 with a $y$ intercept of $-180$ cm$^{-3}$.

## 4. Discussion

Model overpredictions in prior studies are hypothesized to be due to an incomplete characterization of aerosol composition especially in the transition regime between the Aitken and accumulation modes ($D = 50$ to 200 nm). The hypothesis most commonly put forth is an incomplete description of the aerosol composition with a proposed fraction of the aerosol being partially soluble due to the organic fraction. Our study used concurrent measurements of size-resolved aerosol composition from an AMS along with aerosol size–number distribution and CCN number measurements to evaluate this hypothesis. Our results show some overprediction for cases at lower aerosol concentration and a larger overprediction for cases with polluted conditions. Several reasons are plausible for this overprediction including both measurement and modeling biases. On the measurement side, CCN number concentration biases to the low side are theoretically possible due to multiple scattering of the laser beam by droplets at high concentrations. We cannot rule out this possibility from the limited tests performed with the CCN prior to field deployment. Uncertainties in measured supersaturation also exist due to deviations from chamber theory as a result of differences in pad and thermocouple temperature, differences in water vapor over pads compared to pure water, and/or from depletion of water vapor due to aerosol hygroscopic growth at high aerosol number. We performed a series of simulations to estimate the uncertainty in our nominal supersaturations due to vapor depletion. These simulations were performed with the fully coupled version of our model, during which the latent heat released by the growing droplets and water vapor depletion are allowed to affect the supersaturation throughout the chamber. These effects are demonstrated and explored by considering the activation of single-mode aerosol with uniform chemical composition. We varied aerosol number concentrations (from 100 to 5000 cm$^{-3}$) and constrained the lognormal mode size properties from the statistics for case 3, mode 2: $D = 147$, $\sigma = 1.34$. We also performed simulations for an ammonium sulfate case (Van't Hoff factor = 3, molecular weight = 117 g mol$^{-1}$, density = 1777 kg m$^{-3}$) and a hypothetical organic case (Van't Hoff factor = 1, molecular weight = 250 g mol$^{-1}$, density = 1200 kg m$^{-3}$). Figure 11 presents the supersaturation time series during the chamber growth cycle for varying aerosol number concentrations and two particle compositions. Panels (a) and (b) illustrate results for an unperturbed initial supersaturation of 0.197% and 0.450%, respectively. Figure 11 provides an estimate of the uncertainty range introduced in our nominal supersaturation due to vapor depletion. The simulations suggest that significant uncertainty in the

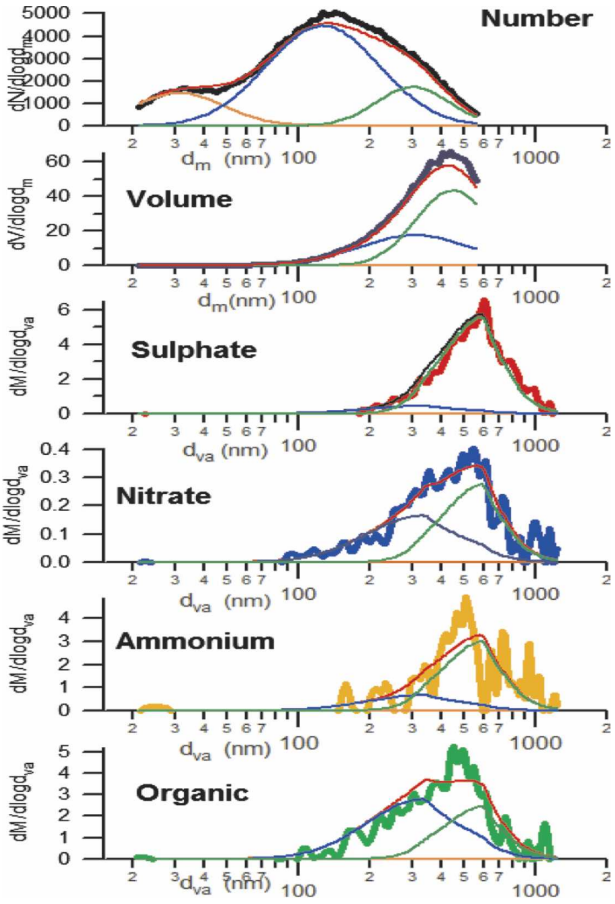


FIG. 8. Observed aerosol size distribution (number, volume, and component mass) with lognormal fits for 0930–1130 EST 16 Jul 2003 (case 1).

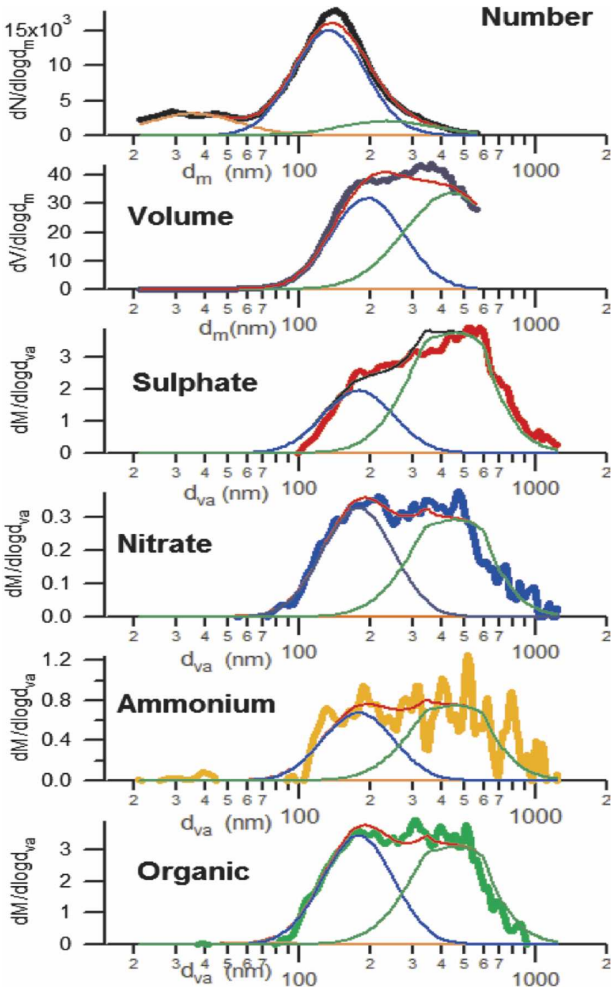


FIG. 9. Observed aerosol size distribution (number, volume, and component mass) with lognormal fits for 1030–1330 EST 17 Jul 2003 (case 2).

instrument supersaturation (hence measured CCN concentrations) exists for aerosol number concentrations greater than 1000 $cm^{-3}$. Recent studies at the University of Wyoming are beginning to address supersaturation calibration uncertainties in a systematic manner (Snider et al. 2003). Here, as described in section 2b, we have applied the recommended corrections to the nominal supersaturation to calculate effective supersaturation, as suggested in Snider et al. (2003). This simple correction is a first attempt to account for the complex behavior in Fig. 11, as it depends on the supersaturation, CCN spectrum, and growth characteristics. We acknowledge that significant uncertainty still exists in our supersaturation estimates and recommend further laboratory studies and model comparisons to better characterize the supersaturation calibration.

We have greater confidence in the measured particle size distributions due to good closure between the long SMPS and the TSI 3022 counter. The long SMPS was also challenged with latex test spheres and was successful in predicting their diameter (within 5%). We also have confidence in the aerosol mass distributions as a result of the duplicate AMS measurements. Good closure for aerosol mass was observed between the long SMPS and the AMS.

A water vapor accommodation coefficient that varied with indicators of pollution could also result in the model–measurement bias at high number concentrations. Here, we performed a best-fit analysis for $\alpha$ by comparing the modeled and measured initial activation curves. We found that a constant value of 0.07 reasonably represented the initial activation curves under different pollution levels. As a result, from our limited number of case studies, we did not find evidence for significant variance in $\alpha$ values with indicators of pollution. Owing to a lack of measurements of size-resolved hygroscopic growth or CCN activation, we are

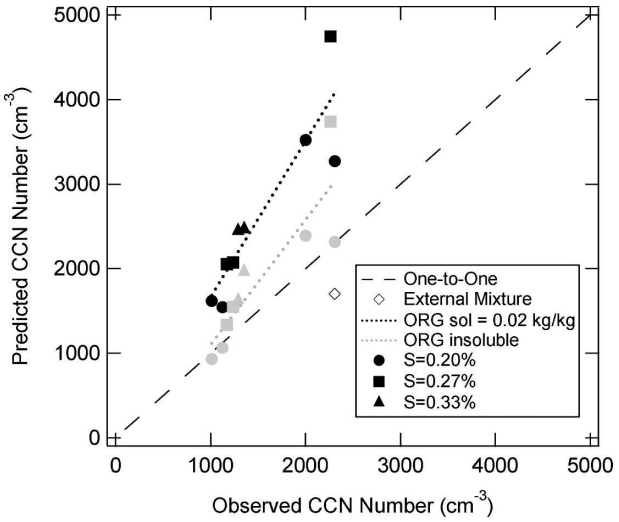


FIG. 10. Comparison between CCN predicted and CCN observed for selected case studies. The symbol type represents chamber supersaturation (circle: 0.20%; square: 0.27%; triangle: 0.33%). The symbol contrast represents sensitivity simulation parameters (dark points for ORG solubility = 0.02 kg kg$^{-1}$; light points for ORG solubility = $1 \times 10^{-5}$ kg kg$^{-1}$). Dashed lines are least squares linear best fits through like contrast points. The open diamond point is the result of a simulation assuming external mixing for mode 2 of case 3.

also assuming in this study that $\alpha$ does not vary significantly across our three lognormal size modes.

An organic aerosol speciation that varied with indicators of pollution could also impact our aerosol–CCN closure. Significant knowledge gaps exist in our understanding of the speciation and physical properties of the organic fraction. Indeed, one of the challenges in this study was assigning an organic aerosol speciation profile for the purposes of calculating the contribution of the organic fraction to particle density, molecular weight, Van't Hoff factor, and solubility. Figure 10 shows the results of series of sensitivity runs assuming an insoluble organic fraction. These sensitivity simulations with an insoluble ORG fraction represent the upper limit for the impact of ORG solubility on CCN concentration. Based on a lack of measurements of water soluble organic fraction in our study, we cannot rule out an insoluble organic fraction as the cause for the model–measurement bias. Indeed, assuming an insoluble organic fraction yield much improved the closure. A best-fit line for the insoluble ORG (lighter line) simulations yielded a slope of 1.5 and $y$ intercept of $-380$ cm$^{-3}$. Future closure studies should include a direct measurement of water soluble organic fraction in the size range critical to CCN activation.

Aklilu (2005) investigated the impact of a two-component ORG soluble model (component 1 with solubility of 0.6 kg kg$^{-1}$ comprising 75% ORG mass and component 2 with solubility of 0.01 kg kg$^{-1}$ comprising 25% ORG mass) on subsaturated growth curves from ambient hygroscopic differential mobility analyzer (H-TDMA) measurements at Egbert, Ontario. Aklilu found a significant improvement in the overall shape of the modeled growth curve compared to measurements between 50% and 90% relative humidity with a two-component ORG model compared to a one-component ORG model. Here, we investigated the impact of two partially soluble ORG components within the CCN chamber model using solubility values similar

TABLE 3. Results from the CCN closure study during CELTIC [duration (EST)/date in July].

| Scenario | Case 1 0930–1130/16 | Case 2 1030–1330/17 | Case 3 2030–2300/17 | Case 4 1745–2000/18 |
|---|---|---|---|---|
| $S$ = 0.20% | | | | |
| Observed | 1011 ± 144 | 1999 ± 168 | 2307 ± 127 | 1123 ± 110 |
| Predicted (ORGsoluble 0.02) | 1621 | 3522 | 3274 | 1546 |
| Predicted (ORG insoluble) | 934 | 2393 | 2319 | 1066 |
| External mixture* | | | 1702 | |
| $S$ = 0.27% | | | | |
| Observed | 1171 ± 134 | 2263 ± 120 | | 1237 ± 98 |
| Predicted (ORGsoluble 0.02) | 2054 | 4745 | | 2076 |
| Predicted (ORG insoluble) | 1337 | 3738 | | 1549 |
| $S$ = 0.33% | | | | |
| Observed | 1291 ± 126 | | | 1352 ± 98 |
| Predicted (ORGsoluble 0.02) | 2444 | | | 2467 |
| Predicted (ORG insoluble) | 1624 | | | 1964 |

* Mode 2 was divided into three external modes (2a, 2b, 2c): one mode being for entirely soluble components (inorganic), one mode for partially soluble components (organic), and one mode being insoluble (elemental carbon). Distribution median diameter and standard deviation for modes 2a, 2b, and 2c were the same as previous mode 2. Total number for modes 2a, 2b, and 2c were calculated by multiplying mass fraction by number for mode 2. Modes 1 and 3 were the same as base case. The summation of number concentration for modes 2a, 2b, and 2c equaled mode 2 (conserved number).

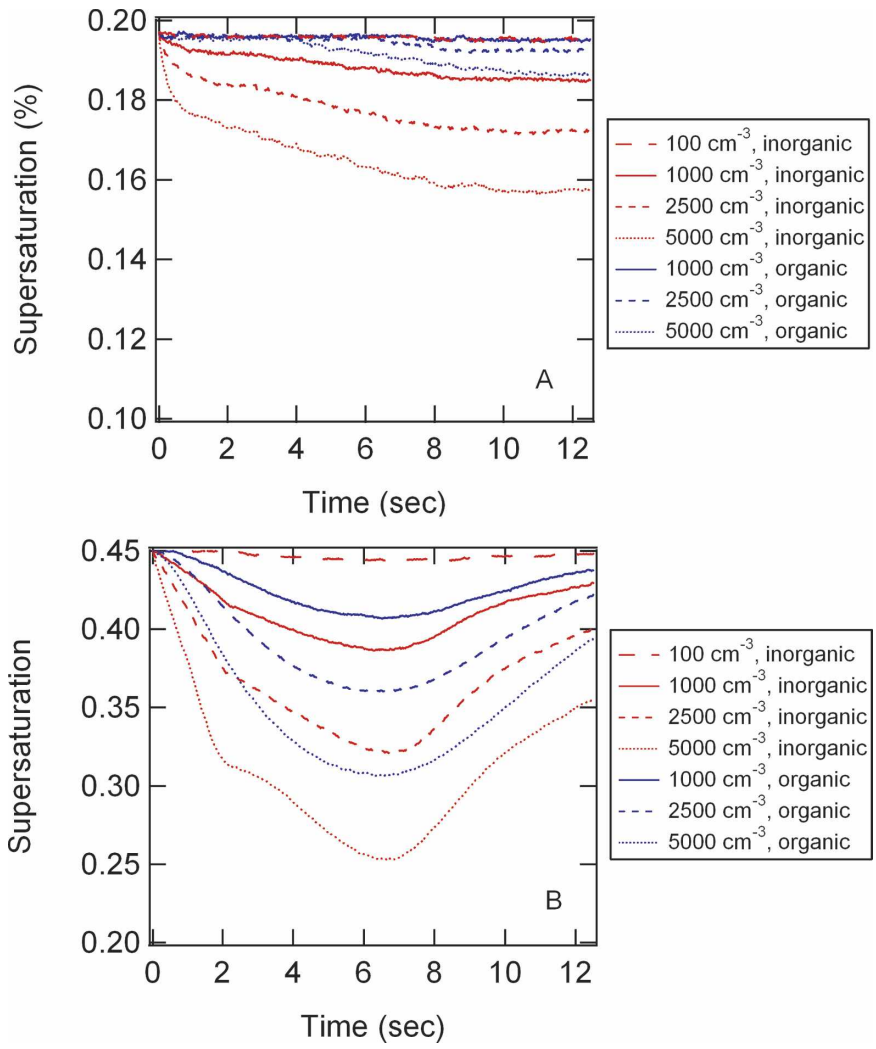


FIG. 11. Modeled supersaturation time series during the chamber growth cycle for varying aerosol number concentration and two particle types (inorganic: Van't Hoff factor = 3, density = 1777 kg $m^{-3}$, molecular weight = 117 g $mol^{-1}$; organic: Van't Hoff factor = 1, density = 1200 kg $m^{-3}$, molecular weight = 250 g $mol^{-1}$). One lognormal size mode with $D$ = 147 nm and $\sigma$ = 1.34 was assumed, initialized with a supersaturation of (a) 0.197% and (b) 0.450%.

to Aklilu (2005). Figure 12 illustrates the predicted supersaturation spectra results for case 1 comparing the two ORG component model with the one ORG component model. A marginal decrease in the CCN concentrations were predicted, but no significant change in slope compared to the one ORG component model. The effect may be small due to the small solubility range to which CCN activation are sensitive (Nenes et al. 2002) and the narrow supersaturation range considered in Fig. 12. An aerosol composition with greater organic fraction may also show a stronger sensitivity to a multicomponent OC model.

The impact of the organic film-forming compounds on aerosol surface tension (Shulman et al. 1996; Facchini et al. 2000) is another area of uncertainty in our modeled results. Here, we assumed aerosol to have the surface tension of a pure liquid water surface. Other studies have identified the sensitivity of CCN concentrations to surface tension depression (Mircea et al. 2002; Nenes et al. 2002; Roberts et al. 2002). Sensitivity results suggest that a 20% decrease in surface tension can increase predicted CCN concentrations by as much as 50% with the effect greatest for small updraft velocities under polluted conditions (Nenes et al. 2002). The lack of surface tension measurements for ambient aerosol limits a more quantitative inclusion in this study.

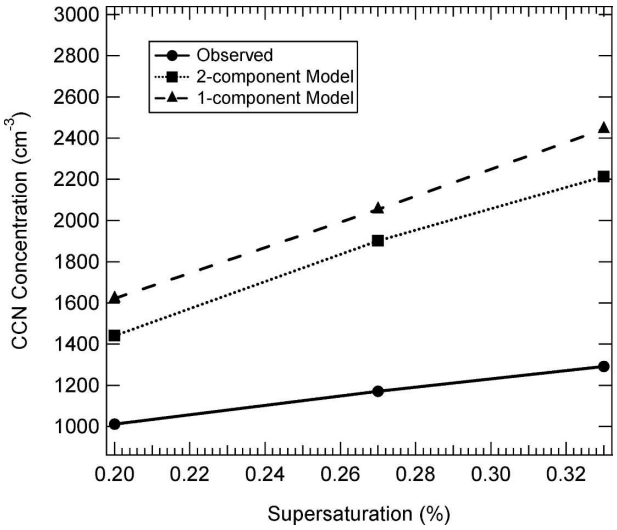


FIG. 12. Observed and predicted CCN supersaturation spectra for case 1 with the one ORG component and two ORG component versions (ORG1 25% by mass, sol = 0.3 kg kg$^{-1}$; ORG2 75% by mass, sol = 0.005 kg kg$^{-1}$) of the chamber model.

However, including the surface tension depression would result in an even larger model–measurement bias. This excludes surface-active compounds as the main cause for the bias.

One final factor that could impact the CCN model–measurement bias is the degree of aerosol external mixing. Multiple aerosol particle types could result from the multitude of emission sources in urban impacted air masses. Three lognormal modes were identified from the SMPS–AMS fitting analysis, each with an internally mixed chemical composition; however, there was not significant overlap of the lognormal modes in diameter. As a result, we describe our distribution as quasi-internally mixed. For example, mode 2 in our analysis is critical in determining modeled CCN concentrations. However, at the distribution median diameters ($D$ = 121 to 147) little overlap is observed with modes 1 and 3. In reality, Aitken and accumulation mode particles with significant differences in particle composition could overlap in this size range. Aitken mode particles are largely organic and insoluble in nature, while accumulation mode particles are internally mixed with inorganic and water soluble and insoluble organic components (Rupakheti et al. 2005). To address whether the uncertainty in mixing state could account for the CCN model–measurement bias we performed a sensitivity simulation by further dividing mode 2 into three externally mixed modes (2a, 2b, and 2c), one mode being completely soluble (inorganics), one mode for partially soluble organics, and one mode for elemental carbon. Distribution median diameter and standard deviation for modes 2a, 2b, and 2c were the same as previous mode 2. Total number for modes 2a, 2b, and 2c were calculated by multiplying volume fraction by number for mode 2. Modes 1 and 3 were the same as base case. The summation of number concentration for modes 2a, 2b, and 2c equaled mode 2 (conserved number). Ambient particle distributions likely fall between the base case internally mixed assumption and the externally mixed sensitivity run. Figure 10 shows the results for this sensitivity run for case 3 at $S$ = 0.2% (open diamond symbol). The CCN prediction showed a large sensitivity to the externally mixed assumption. The assumption introduced by this limiting case did eliminate the model-measurement bias; however a lack of measurements on the ambient aerosol mixing state preclude a more detailed constraint in the model. We recommend direct measurements of aerosol mixing state be added to future aerosol–CCN closure studies [e.g., single particle mass spectrometer (MS) and/or H-TDMA].

## 5. Conclusions

Aerosol sampled at Duke Forest was influenced by a combination of anthropogenic and biogenic sources and, thus, the moderate-to-high pollution conditions provided a stringent test of CCN activation theory. Periods with large Aiken mode number concentrations ($d_m$ = 10–30 nm) due to the impact of local traffic emissions (2000–2100 EST 16 July 2003 and 0624–0724 EST 14 July 2003) and periods with Aiken mode growth to $d_m$ = 70 nm (1739 EST 14 July 2003) did not show increases in observed CCN concentrations. However, a 2-day period with elevated CCN concentrations was observed starting at 0700 EST 17 July 2003 coincident with increases in accumulation mode particle concentrations ($d_m$ = 100–300 nm). These observed differences in CCN concentration stem from the particle size dependence for aerosol activation. Four case studies for further study and CCN prediction were defined within the 2-day pollution period.

CCN predictions require knowledge of numerous ambient aerosol physical properties such as size distribution and mixing state; thermodynamic properties such as solubility, Van't Hoff factor and density; and kinetic parameters such as water-vapor accommodation coefficient. Two novel approaches were developed in this closure study. First, we utilized an SMPS–AMS fitting algorithm to generate three lognormal modes each with unique aerosol size parameters (number concentration, median diameter, distribution standard deviation) and aerosol composition (including organics and inorganics). For the intermediate size mode (mode 2), which is critical in determining CCN number, organic

aerosol fractions for the defined cases were between 58% and 77%. Second, we constrained the water-vapor accommodation coefficient ($\alpha = 0.07$) based on a comparison of our kinetic model with the initial voltage increase observed in the chamber during the activation time period.

Most often, prior aerosol–CCN closure studies have assumed the aerosol to be composed of soluble inorganic material. The model overprediction has been attributed to an incomplete understanding of the aerosol composition, especially the role of organic species in the activation process. This study showed that including measured size resolved aerosol composition (including organic and inorganic fractions) from an AMS along with an assumed organic aerosol speciation profile (pinic acid, fulvic acid, levoglucosan) and an assumed organic solubility (0.02 kg $kg^{-1}$) as input into a kinetic model for CCN activation still resulted in a model overprediction, which was more pronounced for polluted conditions. The overprediction generally does not exceed uncertainty limits, but is indicative that a bias still exists in the measurements or application of model. From this study, we can rule out uncertainties in the particle number and mass size distributions as the cause for the model bias. We are also confident that our model is including the effects of growth kinetics on predicted activated number. However, we cannot rule out uncertainties associated with poorly characterized CCN measurement biases, uncertainties in assumed organic solubility, and uncertainties in aerosol mixing state. We performed a series of simulations to estimate the uncertainty in our nominal supersaturations due to vapor depletion. The simulations suggest that significant uncertainty in the supersaturation exists for aerosol number concentrations greater than 1000 $cm^{-3}$. Furthermore, sensitivity simulations showed that assuming either an insoluble organic fraction or external aerosol mixing were both sufficient assumptions to reconcile the model bias.

*Acknowledgments.* The Duke Forest site was supported by the Office of Science (BER), U.S. Department of Energy, Grant DE-FG02-95ER62083. C. S. would like to acknowledge NCAR's Advanced Studies Program for postdoctoral funding support and Environment Canada for current funding support. Funding for support during the CELTIC field program was provided through the U.S. Environmental Protection Agency. A. N. acknowledges support from a National Science Foundation CAREER award and a Blanchard-Milliken Young Faculty Fellowship. J. L. J. thanks NASA and NSF for support through Grants NNG04GA67G and ATM 0449815 (CAREER), respectively. J. A. H. and P. F. D. are grateful for a NASA Earth Sciences Graduate Fellowship (NGT5-30516) and an EPA STAR Fellowship (FP-91650801), respectively.

## REFERENCES

Aklilu, Y. A., 2005: The hygroscopic properties of atmospheric particles: Influence of composition and atmospheric processes. Ph.D. thesis, York University, 236 pp.

Asa-Awuku, A., and A. Nenes, 2007: The effect of solute dissolution kinetics on cloud droplet formation. *J. Geophys. Res.,* in press.

Barth, M. C., and Coauthors, 2005: Coupling between land ecosystems and the atmospheric hydrologic cycle through biogenic aerosol pathways. *Bull. Amer. Meteor. Soc.,* **86,** 1738–1742.

Cabada, J., S. Pandis, R. Subramanian, A. Robinson, A. Polidon, and B. Turpin, 2004: Estimating the secondary organic aerosol contribution to PM2.5 using the EC tracer method. *Aerosol Sci. Technol.,* **38** (S1), 140–155.

Cantrell, W., G. Shaw, G. R. Cass, Z. Chowdhury, L. S. Hughes, K. A. Prather, S. A. Guazzotti, and K. R. Coffee, 2001: Closure between aerosol particles and cloud condensation nuclei at Kaashidhoo Climate Observatory. *J. Geophys. Res.,* **106** (D22), 28 711–28 718.

Charlson, R. J., J. H. Seinfeld, A. Nenes, M. Kulmala, A. Laaksonen, and M. C. Facchini, 2001: Atmospheric science—Reshaping the theory of cloud formation. *Science,* **292,** 2025–2026.

Chuang, P. Y., 2003: Measurement of the timescale of hygroscopic growth for atmospheric aerosols. *J. Geophys. Res.,* **108,** 4282, doi:10.1029/2002JD002757.

——, D. R. Collins, H. Pawlowska, J. R. Snider, H. H. Jonsson, J. L. Brenguier, R. C. Flagan, and J. H. Seinfeld, 2000: CCN measurements during ACE-2 and their relationship to cloud microphysical properties. *Tellus,* **52B,** 843–867.

Covert, D. S., J. L. Gras, A. Wiedensohler, and F. Stratmann, 1998: Comparison of directly measured CCN with CCN modeled from the number-size distribution in the marine boundary layer during ACE 1 at Cape Grim, Tasmania. *J. Geophys. Res.,* **103** (D13), 16 597–16 608.

DeCarlo, P., J. G. Slowik, D. R. Worsnop, P. Davidovits, and J. L. Jimenez, 2004: Particle morphology and density characterization by combined mobility and aerodynamic diameter measurements. Part 1: Theory. *Aerosol Sci. Technol.,* **38,** 1185–1205.

Delene, D. J., and T. Deshler, 2000: Calibration of a photometric cloud condensation nucleus counter designed for deployment on a balloon package. *J. Atmos. Oceanic Technol.,* **17,** 459–467.

Delia, A. E., 2004: Real-time measurements of non-refractory particle composition and interactions at forested sites. Ph.D. thesis, University of Colorado, Boulder, 180 pp.

Dusek, U., D. S. Covert, A. Weidensohler, C. Neususs, D. Weise, and W. Cantrell, 2003: Cloud condensation nuclei spectra derived from size distributions and hygroscopic properties of the aerosol in coastal south-west Portugal during ACE-2. *Tellus,* **55B,** 35–53.

Facchini, M. C., S. Decesari, M. Mircea, S. Fuzzi, and G. Loglio, 2000: Surface tension of atmospheric wet aerosol and cloud/fog droplets in relation to their organic carbon content and chemical composition. *Atmos. Environ.,* **34,** 4853–4857.

Feingold, G., and P. Chuang, 2002: Analysis of the influence of film-forming compounds on droplet growth: Implications for cloud microphysical processes and climate. *J. Atmos. Sci.,* **59,** 2006–2018.

Fountoukis, C., and Coauthors, 2007: Aerosol–cloud drop concentration closure and droplet formation parameterization evaluation using in-situ data from ICARTT. *J. Geophys. Res.,* in press.

Houghton, J. H., Y. Ding, D. J. Griggs, M. Noguer, P. J. van der Linden, X. Dai, K. Maskell, and C. A. Johnson, Eds., 2001: *Climate Change 2001: The Scientific Basis.* Cambridge University Press, 882 pp.

Jayne, J. T., D. C. Leard, X. Zhang, P. Davidovits, K. A. Smith, C. E. Kolb, and D. R. Worsnop, 2000: Development of an aerosol mass spectrometer for size and composition analysis of submicron particles. *Aerosol Sci. Technol.,* **33,** 49–70.

Jimenez, J. L., and Coauthors, 2003: Ambient aerosol sampling using the aerodyne aerosol mass spectrometer. *J. Geophys. Res.,* **108,** 8425, doi:10.1029/2001JD001213.

Laaksonen, A., P. Korhonen, M. Kulmala, and R. J. Charlson, 1998: Modification of the Kuhler equation to include soluble trace gases and slightly soluble substances. *J. Atmos. Sci.,* **55,** 853–862.

Lance, S., A. Nenes, and T. Rissman, 2004: Chemical and dynamical effects on cloud droplet number: Implications for estimates of the aerosol indirect effect. *J. Geophys. Res.,* **109,** D22208, doi:1029/2004JD004596.

Martin, G. M., D. W. Johnson, and A. Spice, 1994: The measurement and parameterization of effective radius of droplets in warm stratocumulus clouds. *J. Atmos. Sci.,* **51,** 1823–1842.

McFiggins, G., and Coauthors, 2006: The effect of physical and chemical aerosol properties on warm cloud droplet activation. *Atmos. Chem. Phys.,* **6,** 2593–2649.

Meskhidze, N., A. Nenes, W. Conant, and J. H. Seinfeld, 2005: Evaluation of a new cloud droplet activation parameterization with in-situ data from CRYSTAL-FACE and CSTRIPE. *J. Geophys. Res.,* **110,** D16202, doi:10.1029/2004JD005703.

Mircea, M., M. C. Facchini, S. Decesari, S. Fuzzi, and R. J. Charlson, 2002: The influence of the organic aerosol component on CCN supersaturation spectra for different aerosol types. *Tellus,* **54B,** 74–81.

Nenes, A., and J. H. Seinfeld, 2003: Parameterization of cloud droplet formation in global climate models. *J. Geophys. Res.,* **108,** 4415, doi: 10.1029/2002JD002911.

——, P. Y. Chuang, R. C. Flagan, and J. H. Seinfeld, 2001: A theoretical analysis of cloud condensation nucleus (CCN) instruments. *J. Geophys. Res.,* **106** (D4), 3449–3474.

——, R. J. Charlson, M. C. Facchini, M. Kulmala, A. Laaksonen, and J. H. Seinfeld, 2002: Can chemical effects on cloud droplet number rival the first indirect effect? *Geophys. Res. Lett.,* **29,** 1848, doi:10.1029/2002GL015295.

O'Dowd, C. D., and Coauthors, 2004: Biogenically driven organic contribution to marine aerosol. *Nature,* **431,** 676–680.

Otani, Y., and C. S. Wang, 1984: Growth and deposition of saline droplets covered with a monolayer of surfactant. *Aerosol Sci. Technol.,* **3,** 155–166.

Pruppacher, H. R., and J. D. Klett, 2000: *Microphysics of Clouds and Precipitation.* Kluwer Academic, 954 pp.

Raymond, T. M., and S. N. Pandis, 2002: Cloud activation of single-component organic aerosol particles. *J. Geophys. Res.,* **107,** 4787, doi:10.1029/2003JD003503.

Rissler, J., E. Swietlicki, J. Zhou, G. Roberts, M. O. Andreae, L. V. Gatti, and P. Artaxo, 2004: Physical properties of the sub-micrometer aerosol over the Amazon rain forest during the wet-to-dry season transition—Comparison of modeled and measured CCN concentrations. *Atmos. Chem. Phys.,* **4,** 2119–2143.

Rissman, T. A., A. Nenes, and J. H. Seinfeld, 2004: Chemical amplification (or dampening) of the Twomey effect: Conditions derived from droplet activation theory. *J. Atmos. Sci.,* **61,** 919–930.

Roberts, G. C., P. Artaxo, J. Zhou, E. Swietlicki, and M. O. Andreae, 2002: Sensitivity of CCN spectra on chemical and physical properties of aerosol: A case study from the Amazon Basin. *J. Geophys. Res.,* **107,** 8070, doi:10.1029/2001JD000583.

——, A. Nenes, J. H. Seinfeld, and M. O. Andreae, 2003: Impact of biomass burning on cloud properties in the Amazon Basin. *J. Geophys. Res.,* **108,** 4062, doi:10.1029/2001JD000985.

Rubel, G. O., and J. W. Gentry, 1984: Measurement of the kinetics of solution droplets in the presence of adsorbed monolayers: Determination of water accommodation coefficients. *J. Phys. Chem.,* **88,** 3142–3148.

Rupakheti, M., and Coauthors, 2005: An intensive study of the size and composition of submicron atmospheric aerosols at a rural site in Ontario, Canada. *Aerosol Sci. Technol.,* **39,** 722–736.

Seaver, M., J. R. Peele, T. J. Manuccia, G. O. Rubel, and G. Ritchie, 1992: Evaporation kinetics of ventilated waterdrops coated with octadecanol monolayers. *J. Phys. Chem.,* **96,** 6389–6394.

Shantz, N. C., W. R. Leaitch, and P. F. Caffrey, 2003: Effect of organics of low solubility on the growth rate of cloud droplets. *J. Geophys. Res.,* **108,** 4168, doi:10.1029/2002JD002540.

Shulman, M. L., M. C. Jacobson, R. J. Charlson, R. E. Synovec, and T. E. Young, 1996: Dissolution behavior and surface tension effects of organic compounds in nucleating cloud droplets. *Geophys. Res. Lett.,* **23,** 277–280.

Snider, J. R., and J. L. Brenguier, 2000: Cloud condensation nuclei and cloud droplet measurements during ACE-2. *Tellus,* **52B,** 828–842.

——, S. Guibert, J. L. Brenguier, and J. P. Putaud, 2003: Aerosol activation in marine stratocumulus clouds: 2. Kohler and parcel theory closures studies. *J. Geophys. Res.,* **108,** 8629, doi:10.1029/2002JD002692.

Stroud, C. A., and Coauthors, 2002: Nighttime isoprene trends at an urban forested site during the 1999 Southern Oxidant Study. *J. Geophys. Res.,* **107,** 4291, doi:10.1029/2001JD000959.

——, and Coauthors, 2005: Role of canopy-scale photochemistry in modifying biogenic-atmoshere exchange of reactive terpene species: Results from the CELTIC field study. *J. Geophys. Res.,* **110,** D17303, doi:10.1029/2005JD005775.

Turpin, B. J., and H. J. Lim, 2001: Species contributions to PM2.5 mass concentrations: Revisiting common assumptions for estimating organic mass. *Aerosol Sci. Technol.,* **35,** 602–610.

VanReken, T. M., T. A. Rissman, G. C. Roberts, V. Varutbangkul, H. H. Jonsson, R. C. Flagan, and J. H. Seinfeld, 2003: Toward aerosol/cloud condensation nuclei (CCN) closure during CRYSTAL-FACE. *J. Geophys. Res.,* **108,** 4633, doi:10.1029/2003JD003582.

Zhou, J. C., E. Swietlicki, O. H. Berg, P. P. Aalto, K. Hameri, E. D. Nilsson, and C. Leck, 2001: Hygroscopic properties of aerosol particles over the central Arctic Ocean during summer. *J. Geophys. Res.,* **106** (D23), 32 111–32 123.